

Permafrost temperature baseline at the 15 meter-m depth in-on the Qinghai-Tibet Plateau (2010–2019)

Defu Zou¹, Lin Zhao^{2*}, Guojie Hu¹, Erji Du¹, Guangyue Liu¹, Chong Wang², Wangping Li³

¹Cryosphere Research Station on the Qinghai–Tibet Plateau, State Key Laboratory of Cryospheric Science and Frozen Soil Engineering, Northwest Institute of Eco–Environment and Resources, Chinese Academy of Sciences, Lanzhou, 730000, China

²School of Geographical Sciences, Nanjing University of Information Science & Technology, Nanjing, 210044, China

³School of Civil Engineering, Lanzhou University of Technology, Lanzhou, 730050, China

Correspondence to: Lin Zhao (lzhao@nuist.edu.cn)

Abstract. The ground temperature at a fixed depth is a crucial boundary condition for understanding the properties of deep permafrost. However, the commonly used mean annual ground temperature at the depth of the zero annual amplitude ($MAGT_{d_{ZAA}}$ $MAGT_{DZAA}$) has ~~application limitations due to large spatial heterogeneity in observed depths~~ certain limitations for extensive application due to large spatial heterogeneity in observed depths. In this study, we utilized 231 borehole records of mean annual ground temperature at ~~a-the~~ depth of 15 ~~meters-m~~ ($MAGT_{15m}$) from 2010 to 2019 and employed a method of support vector regression (SVR) to predict the gridded $MAGT_{15m}$ at a spatial resolution of nearly 1 km across the Qinghai-Tibet Plateau (QTP). ~~SVR-The SVR model~~ predictions demonstrated ~~a-an~~ R^2 value of 0.48 with a negligible negative overestimation ($-0.01\text{ }^{\circ}\text{C}$). The average $MAGT_{15m}$ of the QTP permafrost was ~~$-1.85\text{ }^{\circ}\text{C}$ ($\pm 1.58\text{ }^{\circ}\text{C}$)~~ $-1.85 \pm 1.58\text{ }^{\circ}\text{C}$, with 90% of values ranging from $-5.1\text{ }^{\circ}\text{C}$ to $-0.1\text{ }^{\circ}\text{C}$ and 51.2% ~~exceeding-greater than~~ $-1.5\text{ }^{\circ}\text{C}$. The ground surface freezing degree days (FDD) was the most significant predictor ($p < 0.001$) of $MAGT_{15m}$, followed by ground surface thawing degree days (TDD), mean annual precipitation (MAP), and soil bulk density (BD) ($p < 0.01$). Overall, the $MAGT_{15m}$ increased from northwest to southeast and decreased with rising elevation. Lower $MAGT_{15m}$ values prevail in high mountainous areas with steep slopes. The $MAGT_{15m}$ was the lowest in the ~~basins-headwater areas~~ of the Amu Darya, Indus, and Tarim ~~rivers~~ (-2.7 to $-2.9\text{ }^{\circ}\text{C}$) river basins (-2.9 to $-2.7\text{ }^{\circ}\text{C}$) and the highest in the ~~Yangtze and Yellow River basins~~ (-0.8 to $-0.9\text{ }^{\circ}\text{C}$) headwater areas of the Yangtze and Yellow river basins (-0.9 to $-0.8\text{ }^{\circ}\text{C}$). ~~The baseline dataset of $MAGT_{15m}$ during 2010–2019 for the QTP permafrost~~ The baseline dataset of $MAGT_{15m}$ for the QTP permafrost regions during 2010–2019 will facilitates simulations of deep permafrost characteristics and provides fundamental data for permafrost model validation and improvement.

Keywords: Mean annual ground temperature; Permafrost; Support vector regression; Qinghai-Tibet Plateau

1 Introduction

The ground temperature at a given depth range is a fundamental indicator for characterizing the thermal state of permafrost (Romanovsky et al., 2010). However, obtaining ~~it-ground temperature~~ at a large depth is challenging due to the harsh climatic

conditions in permafrost regions and time-consuming drilling operations (Zhao et al., 2024). Previous studies have commonly used the mean annual ground temperature (MAGT) at the depth of the zero annual amplitude (DZAA, representing the maximum depth that seasonal surface temperature variations can penetrate) (Dobinski, 2011). Biskaborn et al. (2019) used records of the MAGT at the DZAA (~~MAGT_{dzaa}~~ ~~MAGT_{DZAA}~~), demonstrating that most of the permafrost had experienced warming at a global scale with various magnitudes. The rate of increase in the ~~MAGT_{dzaa}~~ ~~MAGT_{DZAA}~~ is approximately 1 °C per decade in colder permafrost regions in the high-latitude Arctic and 0.3 °C per decade in warmer permafrost in the sub-Arctic regions (Smith et al., 2022).

In addition to indicating permafrost warming at a specific location, the assembled ~~MAGT_{dzaa}~~ ~~MAGT_{DZAA}~~ records can also be utilized to map regional permafrost occurrence using spatialization methods. For instance, Aalto et al. (2018) produced a map of circum-Arctic permafrost based on ~~MAGT_{dzaa}~~ ~~MAGT_{DZAA}~~ derived from statistical forecasting models. However, these maps often do not include permafrost extent to the south of 30°N in the Northern Hemisphere. Although the European Space Agency (ESA) Climate Change Initiative (CCI) provides permafrost MAGT products for the Northern Hemisphere (Obu et al., 2021), the deepest depth reached is only 10 ~~meters-m~~, limiting the applicability to regions where the DZAA exceeds 10 ~~meters-m~~, such as the Qinghai-Tibet Plateau (QTP). Recently, Ran et al. (2022) updated the Northern Hemisphere permafrost map by incorporating more observed ~~MAGT_{dzaa}~~ ~~MAGT_{DZAA}~~ data from the QTP and ~~northeast~~ ~~Northeast~~ China and employing multiple machine-learning models, demonstrating significant advancements in mapping permafrost distribution and thermal state.

A critical consideration is the DZAA variability across different regions because it depends on permafrost dynamics. Measurements from 1002 boreholes have shown that the DZAAs ~~ranged-range~~ from approximately 3 to 25 ~~meters-m~~ in different permafrost regions (Ran et al., 2022). The DZAAs are typically shallower in peat and mineral soils and deeper in bedrock (Smith et al., 2010). The DZAAs generally range from 10 to 15 ~~meters-m~~ in ~~central~~ ~~Central~~ Asia, depending on surface land cover and substrate properties (Zhao et al., 2010). Furthermore, DZAAs undergo change with permafrost warming, as evidenced by ~~in-situ-in situ~~ observations indicating a decrease rate of 0.14-0.17 ~~meters-m~~ per year near ~~the northern permafrost limit~~ ~~the northern limit of elevational permafrost~~ on the QTP from 2005 to 2017, leading to consequent changes in ~~MAGT_{dzaa}~~ ~~MAGT_{DZAA}~~ (Liu et al., 2021). The spatial and temporal variability of DZAAs complicates the use of the predicted ~~MAGT_{dzaa}~~ ~~MAGT_{DZAA}~~ maps for comparison and calibration with transient modeling results at specific depths and also limits their utility in estimating ~~deeper-permafrost characteristics~~ ~~deeper characteristics of permafrost at greater depths~~ (e.g., permafrost thickness). Hence, establishing a baseline of MAGT at a specific depth and for a specific period is crucial for permafrost modeling studies.

The QTP ~~is-has~~ the largest permafrost region in low and mid-latitudes and a typical high-altitude permafrost area (Zou et al., 2017). ~~Over the past two decades, permafrost monitoring efforts on the QTP have established a substantial monitoring network and some datasets have been published (Zhao et al., 2021).~~ ~~Over the past two decades, permafrost monitoring efforts on the QTP have established a substantial monitoring network and some datasets have been published (Zhao et al., 2021).~~ Particularly

since 2010, extensive monitoring has been conducted by various research groups in multiple regions, resulting in updated datasets. ~~This study aims to establish a fixed-depth deep permafrost temperature baseline using data from the QTP for the last decade (2010-2019) and a machine learning approach to address the limitations associated with the use of MAGT_{dzaa}. MAGT data at 15 meters depth are used for spatialization, considering that DZAAs generally ranges from 10 to 15 meters in the QTP (Zhao et al., 2010).~~ This study aims to establish a fixed-depth deep permafrost temperature baseline using data from the QTP for a decade (2010-2019) and a machine learning approach to address the limitations associated with the use of MAGT_{DZAA}. Considering the availability of ground temperature records, the data of MAGT at 15 m in depth are used for spatialization. The resulting dataset can serve as a reference for model simulations during this period and provide an upper boundary condition for estimating ~~deeper permafrost characteristics~~ characteristics of permafrost at greater depths.

2 Materials and Methods

2.1 Compilation and Processing of MAGT Data

The dataset of mean annual ground temperature at 15 m in depth (MAGT_{15m}) across the QTP permafrost ~~region~~ regions consisted of a total of 231 boreholes (Fig. 1). For this dataset, 122 measurements were obtained from the permafrost monitoring networks of the QTP (Zhao et al., 2021) established by the Cryosphere Research Station, Chinese Academy of Sciences (CRS-CAS). The ~~remaining-rest~~ 109 measurements were compiled from published articles (Cao et al., 2018; Li et al., 2012, 2014, 2016; Luo et al., 2012, 2013, 2018; Sun et al., 2018; Liu and Shi, 2019). The observational period was from 2010 to 2019. The ground temperature in the boreholes was measured using a cable equipped with a string of thermistors at various depths. The thermistor probe was ~~developed-assembled~~ and calibrated by the State Key Laboratory of Frozen Soil Engineering (SKLFSE, CAS), ~~ensuring-with~~ a measurement accuracy of ± 0.05 °C in laboratory conditions (Wu et al., 2010). All ground temperature measurements were obtained using the same equipment, ensuring the comparability of MAGT_{15m} across various permafrost regions.

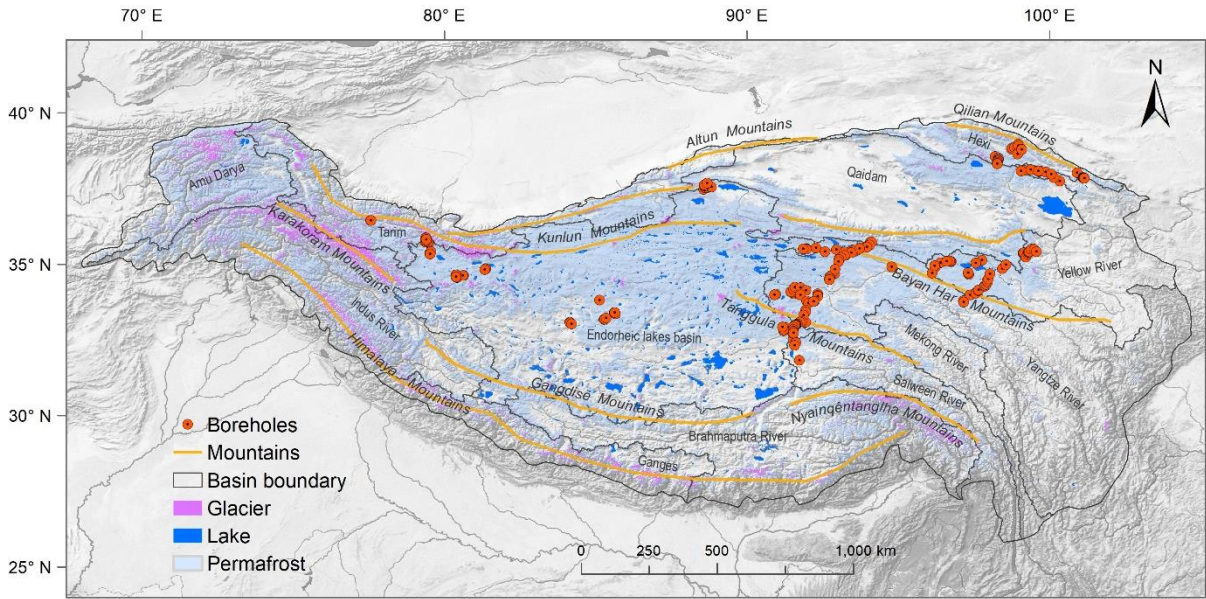
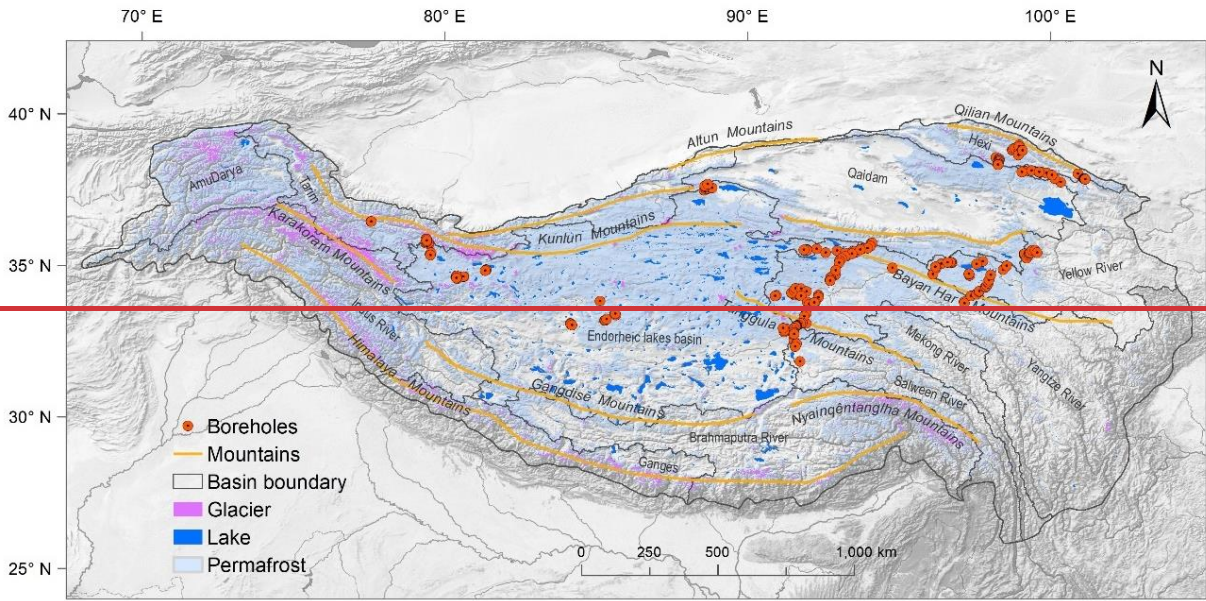
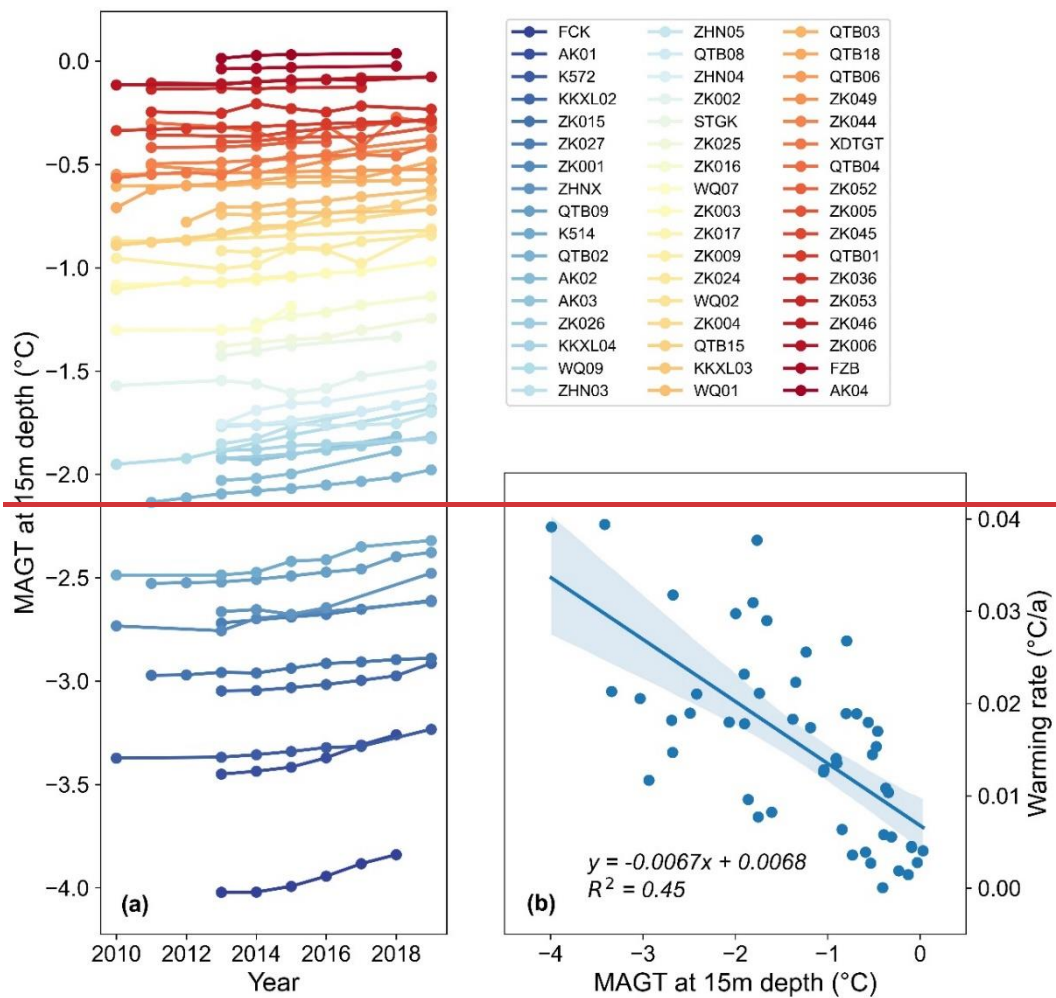


Figure 1: Distribution of boreholes (n=231) for monitoring mean annual ground temperature at 15 m in depth (MAGT_{15m}) on the Qinghai-Tibet Plateau.

Of the 231 boreholes, 180 sites (approximately 78%) only had single-year observations. To ensure that each site had values for each year from 2010 to 2019, we implemented the following processes:

90 1) For sites with multiple years of MAGT_{15m} observations, we calculated the warming rates from 2010 to 2019 (Fig. 2a) and
established the linear relationship between the warming rates and the average MAGT_{15m} (2010-2019) (Fig. 2b). A rigorous
selection process was used for sites with a minimum requirement of three observation years and a time span of six years. This
selection criterion ensured that the chosen sites provided a robust basis for calculating the warming rate. Consequently, 51
sites were included in the analysis. The MAGT_{15m} range for these sites was -3.95 °C to 0.03 °C, encompassing a diverse
95 temperature range in the dataset.



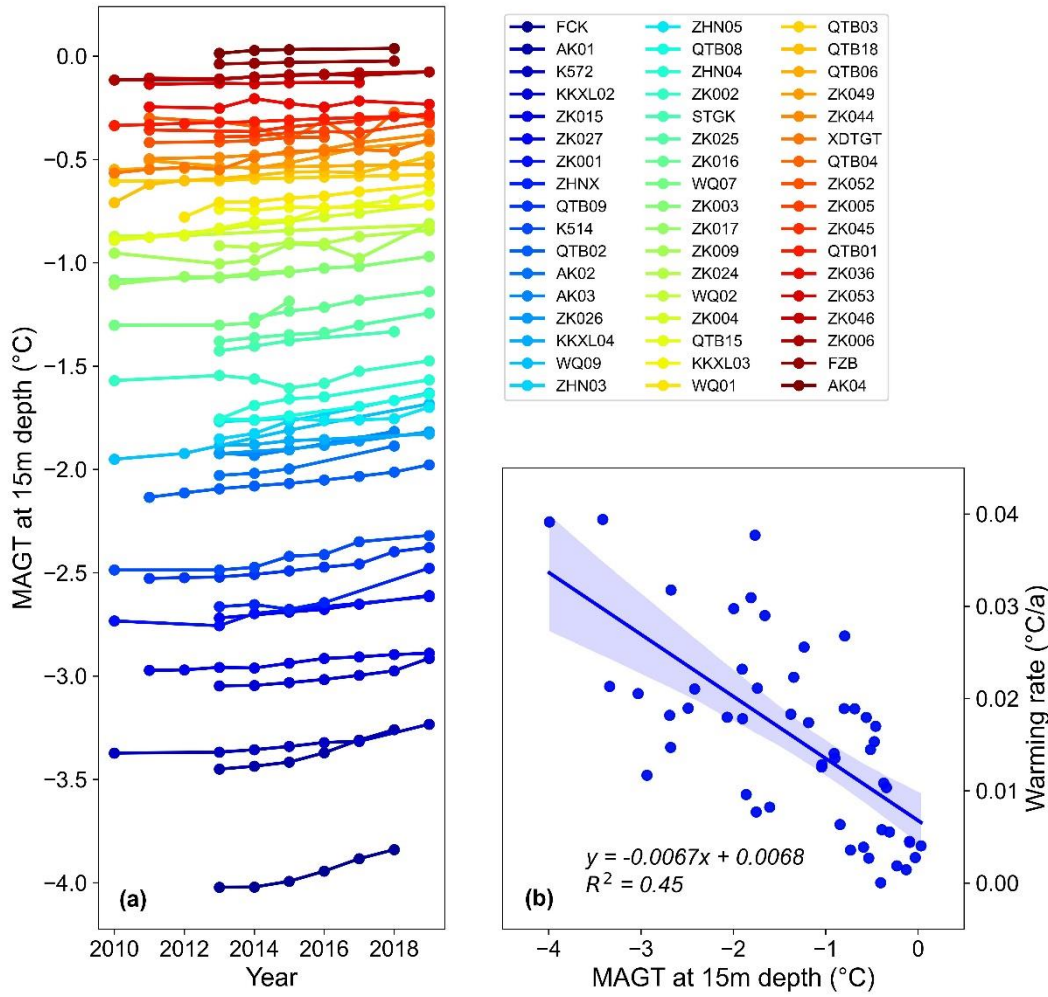


Figure 2: Warming rates of $MAGT_{15m}$ during 2010-2019 (a) and the relationship between warming rates and the average $MAGT_{15m}$ (b).

2) For sites that did not meet the first criterion, i.e., sites with observation years of less than three years or a time span of less than six years (a total of 180 sites), we used the following linear relationship (Equation 1) to fill-estimate in the missing values.

$$MAGT_{15m} \text{ warming rate} = -0.0067 \times MAGT_{15m} + 0.0068 \quad (R^2 = 0.4549) \quad (1)$$

where, the $MAGT_{15m}$ warming rate represents the rate of warming of-in $MAGT_{15m}$ from 2010 to 2019, and $MAGT_{15m}$ is the mean $MAGT$ value at a depth of 15 m from 2010 to 2019.

After obtaining the yearly $MAGT_{15m}$ values for all sites from 2010 to 2019, we computed the mean $MAGT_{15m}$ value during the ten years. It was used as the input for regional $MAGT_{15m}$ predictions. This approach ensured the integration of long-term trends and provided a representative estimate of the regional $MAGT$.

2.2 Statistical Learning Model

In this study, ~~we employed the~~ support vector regression (SVR) method (Basak et al., 2007) was adopted to predict the MAGT_{15m}. Although several machine learning models, including generalized linear model (GLM), generalized additive model (GAM), random forest (RF), and geographically weighted regression (GWR), have been commonly used in various regression analyses (Aalto et al., 2018; Wang et al., 2020; Ran et al., 2022), the SVR method has demonstrated better performance for predicting the MAGT in the QTP permafrost ~~region~~ regions compared to other methods (Ran et al., 2021). Moreover, SVR is a deterministic prediction method, ensuring consistent and reproducible results for a fixed set of sample points, contributing to the reliability and replicability of predictions.

The SVR was implemented using the R package e1071. SVR is a nonparametric technique that seeks to find a function deviating from observations by a value not exceeding a threshold (ϵ) for the training points while minimizing the prediction error. ~~The output model depends on kernel functions, the default radial kernel function was utilized in this study. The output model depends on kernel functions. Thus, the default radial kernel function has been utilized in this study.~~ Model parameter selection was performed using a tuning method, with a cost parameter of 1000 employed to prevent overfitting and a gamma value of 0.0001. Model performance was assessed using the bias, root-mean-square error (RMSE), and coefficient of determination (R^2) computed ~~via-via~~ 10-fold cross-validation with 1000 ~~repetitions~~ iterations. In each run, 90% of the measurements were used to train the SVR model, ~~while the remaining 10% were used to test predictions~~ while the remaining 10%, to test predictions.

2.3 Environmental and Climate Data

Nine environmental and climate variables were selected as predictors in the prediction of MAGT_{15m} using the SVR method. They were selected based on previous studies (~~e.g.~~, Aalto et al., 2018; Ran et al., 2021), and these variables were derived from high-quality datasets available at present (~~see~~ Table 1).

Volumetric coarse fragments (CF, %) and bulk density (BD, g/cm³) in the soils were obtained from the SoilGrids 2.0 data (Poggio et al., 2021) with a spatial resolution of 1 ~~km by~~ x 1 km. In addition to soil texture, soil organic carbon content (SOC, g/kg) data from the Third Pole (Wang et al., 2021) was also used. Average values for a depth range of 0-2 m were used for all soil factors as model inputs. The number of freezing degree days (FDD, °C-days) and thawing degree days (TDD, °C-days) based on ground surface temperature (GST) were calculated following the method of Zou et al. (2017), and the data period was expanded to 2003-2019. GST, corrected based on MODIS LST, was selected in this study due to its superior performance over air temperature in permafrost modeling (Luo et al., 2018). Mean annual precipitation (MAP, mm) from 1970 to 2000 was derived from the WorldClim version 2.1 dataset (Fick and Hijmans, 2017). Snow cover duration (SCD, days) from 2003 to 2020 was derived from the MODIS daily cloud-free snow cover product (Qiu et al., 2021). The multi-year averages of FDD, TDD, MAP, and SCD were calculated and used as model inputs. The elevation was obtained from a dataset compiled by

Amatulli et al. (2018). The multi-year averaged maximum value of the normalized difference vegetation index (NDVI) from 2000 to 2021 was derived from the MOD13A2 products (Wang et al., 2022).

Table 1. Environmental predictors used in the modeling.

Predictor	Unit	Data Source
Coarse fragments (CF)	%	Poggio et al., 2021 (SoilGrids 2.0)
Bulk density (BD)	g/cm ³	
Soil organic carbon content (SOC)	g/kg	Wang et al., 2021
Freezing degree days (FDD)	°C-days, average for 2003–2019	expanded the data of Zou et al., 2017
Thawing degree days (TDD)	°C-days, average for 2003–2019	
Mean annual precipitation (MAP)	mm, average for 1970-2000	Fick and Hijmans, 2017 (WorldClim version 2.1)
Snow Cover Duration (SCD)	days, average for 2003-2020	Qiu et al., 2021
Elevation (DEM)	m	Amatulli et al., 2018
Normalized difference vegetation index (NDVI)	maximum value in a year, average for 2000-2021	Wang et al., 2022 (MOD13A2 products)

2.4 Ancillary Data

Prior to calculating statistics, the SVR predictions were resampled to a spatial resolution of 1 km by 1 km. Additionally, areas covered by glaciers and lakes were masked from the output results. Glacier areas were masked using the Randolph Glacier Inventory (RGI6.0) data obtained from the National Snow and Ice Data Center (<https://nsidc.org/data/nsidc-0770/versions/6>). Lake areas were masked by referencing the dataset of "the lakes larger than 1 km² in the Tibetan Plateau (v3.1) (1970-2022)" (Zhang et al., 2019) provided by the National Tibetan Plateau Data Center (<http://data.tpdc.ac.cn/>).

3 Results

3.1 Model Performance

~~The cross validation of 1000 runs demonstrated that the SVR model achieved high accuracy. The mean values of the three statistical indicators, i.e., bias, root mean square error (RMSE), and coefficient of determination (R^2) were $-0.01\text{ }^{\circ}\text{C}$ ($\pm 0.11\text{ }^{\circ}\text{C}$), $0.71\text{ }^{\circ}\text{C}$ ($\pm 0.13\text{ }^{\circ}\text{C}$), and 0.48 (± 0.14), respectively. The cross-validation of 1000 runs demonstrated that the mean values of the three statistical indicators, i.e., bias, root-mean-square error (RMSE), and coefficient of determination (R^2) were $-0.01\text{ }^{\circ}\text{C}$ ($\pm 0.11\text{ }^{\circ}\text{C}$), $0.71\text{ }^{\circ}\text{C}$ ($\pm 0.13\text{ }^{\circ}\text{C}$), and 0.48 (± 0.14), respectively.~~ Figure 3 shows the scatterplot depicting the relationship between the predicted ~~MAGT_{15m} values and the observed measurements~~ and observed MAGT_{15m} values. The fitted line is close to the 1:1 line, with a bias and RMSE of $0.01\text{ }^{\circ}\text{C}$ and $0.73\text{ }^{\circ}\text{C}$, respectively, indicating a close agreement with the cross-validation results. The predictions exhibited slight underestimations at high MAGT_{15m} values, while overestimations at lower ground temperatures ones.

Multilinear regression analysis revealed that the contribution of FDD to the $MAGT_{15m}$ prediction was highly significant (p<0.001), whereas those of the TDD, MAP, and BD were significant (p<0.01). However, the contributions of the remaining five factors (DEM, SCD, SOC, CF, and NDVI) were insignificant. Overall, at the plateau scale, the ground surface temperature (especially for FDD), precipitation, and soil bulk density contributed the most to $MAGT_{15m}$, whereas the other environmental and climate factors modified this influence at the regional scale.

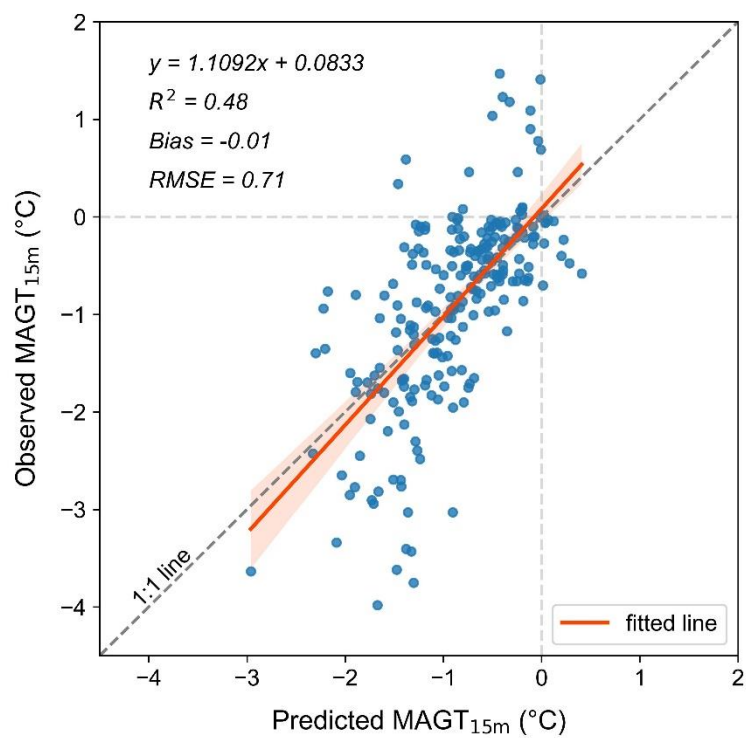
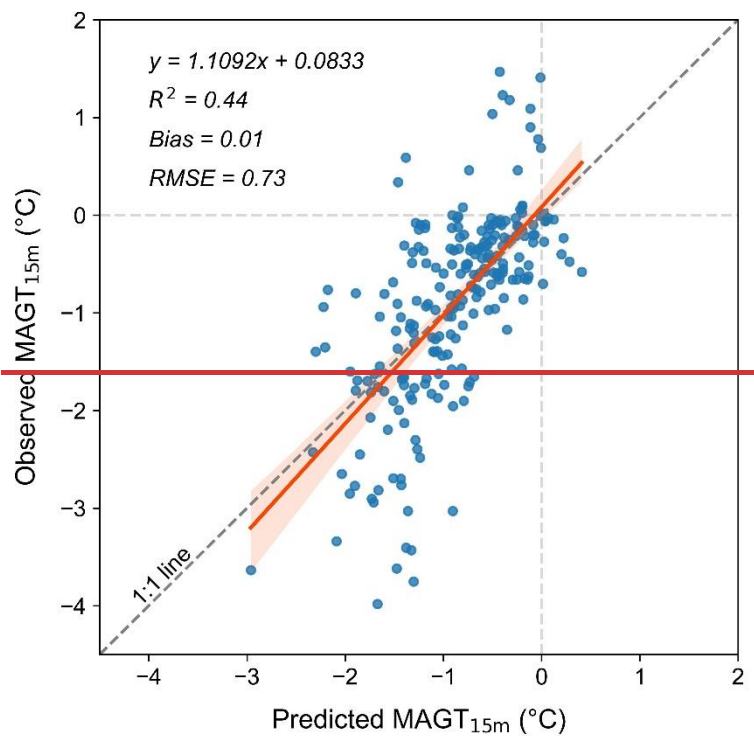


Figure 3: Relationship between predicted and observed mean annual ground temperatures at 15 m depth (MAGT_{15m}) in permafrost regions on the Qinghai-Tibet Plateau during 2010-2019.

3.2 Distribution-Distributive Characteristics

3.2.1 General distribution characteristics of MAGT_{15m}

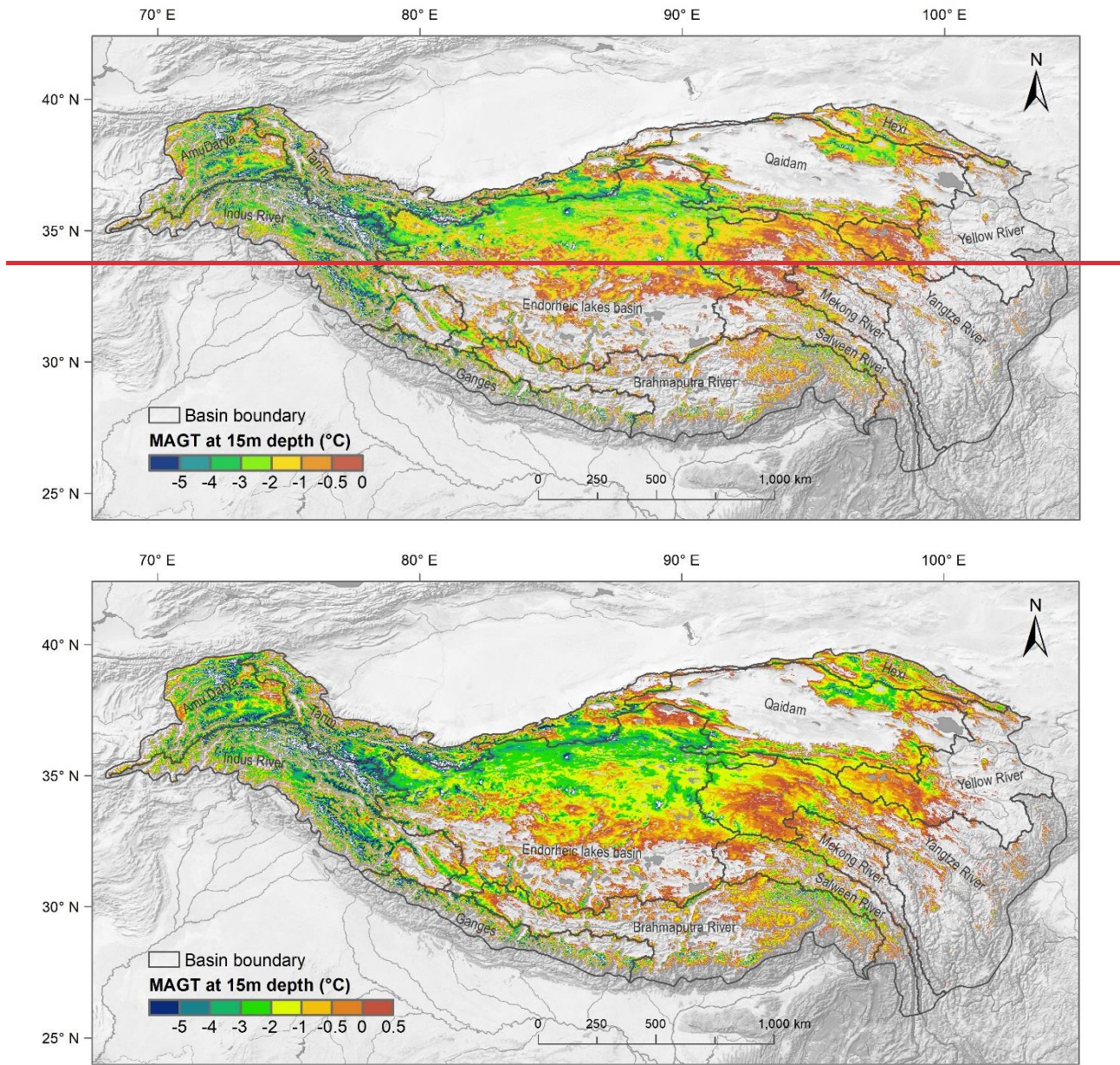
170 Figure 4 illustrates the spatial distribution ~~pattern-patterns~~ of the predicted MAGT_{15m} ~~in-on~~ the QTP for the period 2010-2019. Overall, the MAGT_{15m} exhibited ~~an increasing trend from northwest to southeast spatially~~ a southeastward increasing trend. Regions with the lowest MAGT_{15m} ~~values~~ (depicted as dark blue in Fig. 4) were primarily located in the high mountain regions of the western QTP, e.g., the western Kunlun, Karakoram, and western Himalaya mountains (as displayed in Fig. 1). Regions with lower MAGT_{15m} values were predominantly found in the central Kunlun, Tanggula, and Qilian mountains of the northern

175 QTP. ~~The~~ MAGT_{15m} increased south- and eastward, with high values concentrated in the majority of the Yangtze and Yellow ~~source areas~~ rivers source areas, as well as the southern areas of the ~~Endorheic~~ endorheic lakes basin. In other high mountainous regions, such as the Altun, Gangdise, eastern Himalayas, and Nyainqêntanglha mountains, MAGT_{15m} ~~changed-lowered~~ rapidly over short distances due to the steep mountainous terrain.

The ~~region-regions~~ with negative MAGT_{15m} values covered an area of 1.36×10^6 km² (excluding glacier and lake areas),

180 accounting for approximately 44.0% of the total QTP area. ~~The average MAGT_{15m} was -1.85 °C with a standard deviation of ± 1.58 °C, and 90% of the values ranged from -5.1 °C to -0.1 °C. The average MAGT_{15m} was -1.85 ± 1.58 °C, and 90% of the~~ MAGT_{15m} values ranged from -5.1 to -0.1 °C. The zoning statistics of ~~the temperature-MAGT_{15m}~~ indicated that the area with extremely low values was relatively small. The area with MAGT_{15m} ~~values~~ below -5 °C was 0.07×10^6 km², accounting for only 5.1% of the ~~region-regions~~ with negative MAGT_{15m} ~~values~~. The areas with MAGT_{15m} ~~values~~ below -3 °C was 0.25×10^6

185 km², representing 18.1% of the ~~region-regions~~ with negative MAGT_{15m} ~~values~~. The areas for the ~~temperature-MAGT_{15m}~~ ranges of -3 to -2 °C, -2 to -1 °C, and -1 to 0 °C were 0.24 , 0.38 , and 0.49×10^6 km², accounting for 17.8%, 28.0%, and 36.1%, respectively.

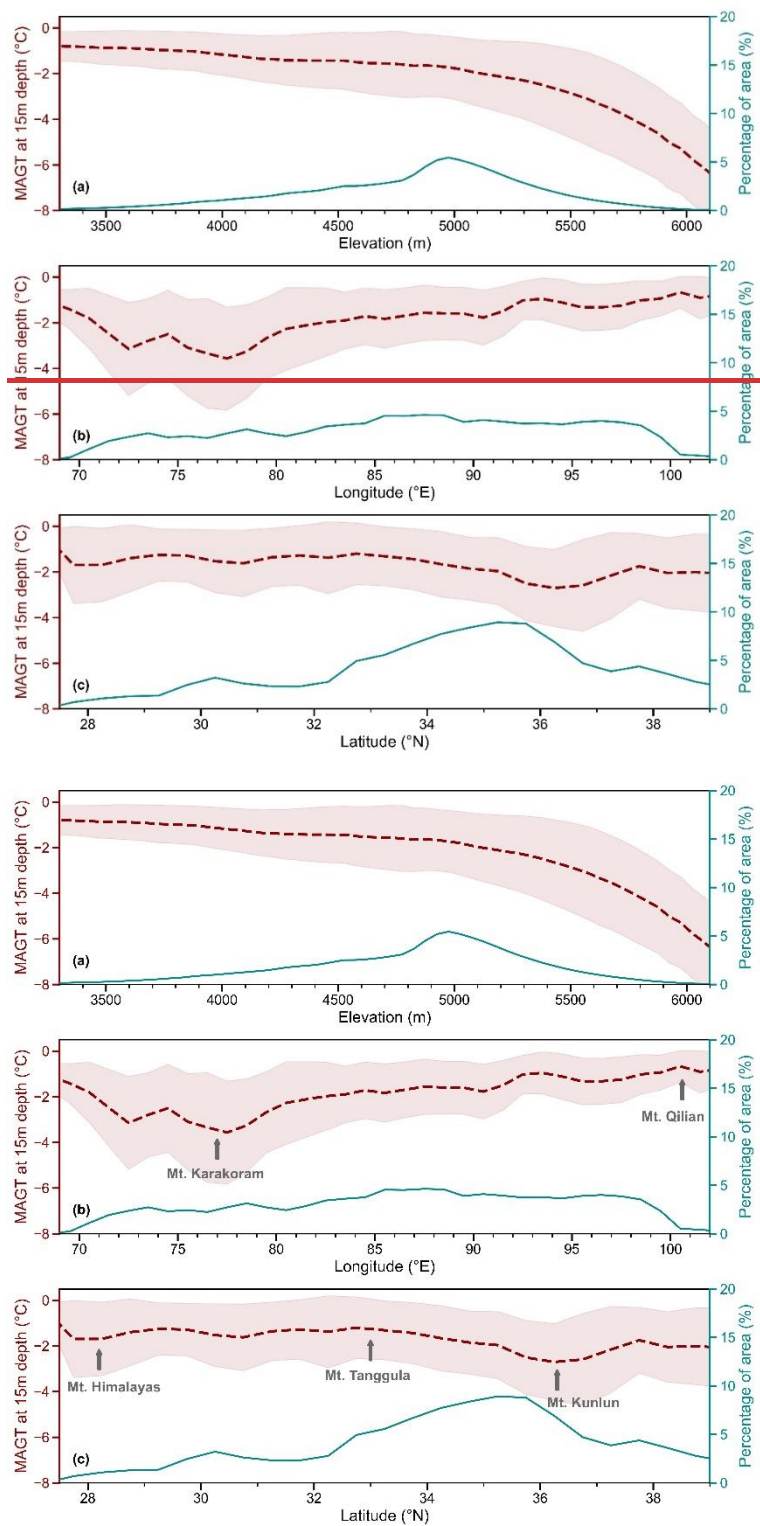


190 **Figure 4: Spatial distribution of predicted mean annual ground temperatures at the 15m depth (MAGT_{15m}) across the Qinghai-Tibet Plateau during 2010-2019.**

The three-dimensional ground thermal states across the QTP were investigated based on the predicted MAGT_{15m}. Figure 5a illustrates the distribution of the MAGT_{15m} at different elevations and the percentage of area. Area analysis reveals that approximately 90% of the MAGT_{15m} values fell in the elevation range of 3840 to 5570 m a.s.l. Generally, ~~the~~ MAGT_{15m} 195 demonstrated a decreasing trend as elevation increased, and the variability in MAGT_{15m} ~~values~~ was more pronounced at higher

elevations and less significant at lower elevations. Meanwhile, the lapse rate of MAGT_{15m} was relatively low at lower elevations and increased as the elevation rises.

The MAGT_{15m} in the west-to-east longitudinal transect increased ~~monotonically-monotonously~~ (Fig. 5b). The western regions of the plateau exhibited the lowest MAGT_{15m} values (e.g., approximately -3 °C in the longitude range of 72°E to 78°E), whereas the easternmost areas had the highest values (approximately -1°C to the east of 100°E). Concurrently, the amplitude of the temperature variations gradually declined ~~as the MAGT_{15m} values increased from west to east with the eastward rising~~ MAGT_{15m}. Figure 5c illustrates the MAGT_{15m} trend in the latitudinal transect. The regional average MAGT_{15m} was generally stable at approximately -1.5 °C from 28°N in the Himalayas to 33°N in the Tanggula Mountains. ~~The~~ MAGT_{15m} decreased slightly from 33°N northwards, and the average was lower than in areas south of 33°N. The lowest latitudinal MAGT_{15m} values occurred near 36°N, primarily in the ~~regions of~~ Kunlun and Karakoram ~~regions mountains~~.



210

Figure 5: Variations of mean annual ground temperature at 15m depth (MAGT_{15m}) along elevation (a), longitude (b), and latitude (c) transects in-on the Qinghai-Tibet Plateau (the dashed red line represents the mean MAGT_{15m}, and the light-red shaded area indicates its standard deviation; the cyan dashed line shows the percentage-of-area areal percentage).

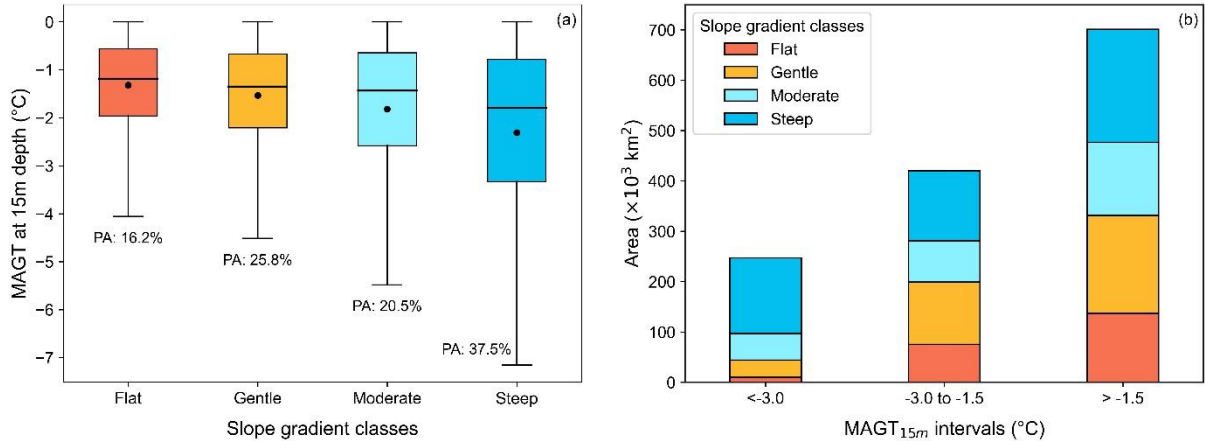
215

Due to the predominant mountainous and high-plateau-high-plateau terrain of the QTP, we utilized slope as a topographical indicator to assess the spatial distribution characteristics of the MAGT_{15m}. Considering the slope distribution pattern within the study areas, we aggregated the slope gradients into four classes: flat (slope < 2°), gentle (2-2° to 8°), moderate (8-8° to 17°), and steep (> 17°). Statistical analysis reveals that the percentage of area (PA, %) of flat, gentle, and moderate slopes was 16.2%, 25.8%, and 20.5%, respectively. Regions with steep slopes comprised a significant portion, with a PA of 37.5% (Fig. 6a). Overall, the average MAGT_{15m} exhibited a decreasing trend as the slope increased, indicating that lower MAGT_{15m} values were more prevalent in areas with steeper slopes (e.g., high mountainous regions of the QTP).

220

Additionally, we analyzed the distribution of the four slope classes in three MAGT_{15m} intervals: low (< -3 °C), medium (-3 to -1.5 °C), and high (> -1.5 °C) (Fig. 6b). The areas of low-, medium-, and high-temperature regions were 24.5, 41.6, and 69.5×10⁴ km², accounted for 18.1%, 30.7%, and 51.2%, respectively. Most of the MAGT_{15m} values in the low-temperature interval were concentrated in regions with steep slopes and accounting for 60.6% of the total area. The areas of moderate slopes account for 21.4%, and the combined areas of flat and gentle slopes represented only 18.0% of the total. The areas of flat, gentle, moderate, and steep slopes accounted for 17.9%, 29.5%, 19.5%, and 33.1% in the medium-temperature interval and for 19.6%, 27.7%, 20.7%, and 32.0% in high-temperature interval, respectively, indicating similar proportions. Moreover, the areas of flat and gentle slopes were predominant in the medium- and high-temperature intervals, representing more than half of the total area in each interval. Topographically, MAGT_{15m} values in high- and medium-temperature intervals (i.e., MAGT_{15m} > -3 °C) occurred substantially in areas with flat and gentle slopes, whereas low-temperature regions were rare on these slopes.

225



230

Figure 6: Mean annual ground temperature at 15 m depth (MAGT_{15m}) for different slope gradients on the Qinghai-Tibet Plateau during 2010-2019 (PA: percentage of area).

3.2.2 Regional distribution characteristics of MAGT_{15m}

To explore the spatial variability in different regions, we conducted the zonal statistics of the MAGT_{15m} for 12 primary river or lake basins ~~in-on~~ the QTP (Fig. 7). ~~Figure-Figures~~ 7a and 7b show the box plots and cumulative plots of the three temperature intervals (~~$<-3^{\circ}\text{C}$, -3 to -1.5°C , and $>-1.5^{\circ}\text{C}$~~) (~~<-3 , -3 to -1.5 , and $>-1.5^{\circ}\text{C}$~~) of ~~the~~ MAGT_{15m} in ~~the-these~~ basins, respectively. Figure 7 is organized primarily from west to east based on the location of the basins, showing an overall increasing trend in ~~the~~ MAGT_{15m}, consistent with the longitudinal profile results (Fig. 5b).

The lowest MAGT_{15m} values were observed in the ~~basins-headwater areas~~ of the Amu Darya, Indus, and Tarim ~~river-river~~ ~~basins~~ in the western QTP, with average MAGT_{15m} values of -2.69°C , -2.93°C , and -2.80°C , respectively. These three basins also exhibited the largest standard deviations, ranging from ± 1.89 to $\pm 2.11^{\circ}\text{C}$. Low MAGT_{15m} values occurred throughout these basins, with areas of MAGT_{15m} $< -3^{\circ}\text{C}$ comprising 37.7% to 42.4% and those $< -5^{\circ}\text{C}$ comprising 12.0% to 17.0% of the total basin area. Another region with low MAGT_{15m} ~~values~~ and high ~~variations-variability~~ was the Ganges River basin on the ~~southernmost-southern~~ QTP. The mean MAGT_{15m} was ~~$-2.30^{\circ}\text{C} (\pm 1.84^{\circ}\text{C})$~~ $-2.30 \pm 1.84^{\circ}\text{C}$, and areas of MAGT_{15m} $< -3^{\circ}\text{C}$ and $< -5^{\circ}\text{C}$ comprised 31.4% and 10.1% of the total basin area, respectively.

The average MAGT_{15m} ~~value~~ in the ~~Endorheic Lakes'-basin-endorheic lakes basin~~ was -1.73°C , higher than ~~that~~ in the western basins, with a small standard deviation of $\pm 1.17^{\circ}\text{C}$. This result indicates minimal spatial ~~variation-variability~~ in MAGT_{15m} ~~values~~, despite the basin being the most extensive permafrost area of the QTP. Few low MAGT_{15m} values were observed in this basin, accounting for only 12.1% and 1.4% of areas with MAGT_{15m} $< -3^{\circ}\text{C}$ and $< -5^{\circ}\text{C}$, respectively. The Brahmaputra River basin exhibited the highest mean MAGT_{15m} among the western and central QTP basins, reaching ~~-1.31°C with a small deviation of $\pm 1.21^{\circ}\text{C}$~~ $-1.31 \pm 1.21^{\circ}\text{C}$.

The six river basins ~~in-on~~ the eastern QTP generally exhibited higher MAGT_{15m} ~~values~~ with smaller fluctuations. The Qaidam and Hexi basins ~~in-on~~ the northeastern QTP had lower MAGT_{15m} values of ~~$-1.59^{\circ}\text{C} (\pm 1.19^{\circ}\text{C})$ and $-1.44^{\circ}\text{C} (\pm 1.11^{\circ}\text{C})$~~ $-1.59 \pm 1.19^{\circ}\text{C}$ and $-1.44 \pm 1.11^{\circ}\text{C}$, respectively. ~~In-On~~ the southeastern QTP, the Salween and Mekong ~~river~~ basins exhibited MAGT_{15m} values of ~~$-1.09^{\circ}\text{C} (\pm 0.93^{\circ}\text{C})$ and $-0.91^{\circ}\text{C} (\pm 0.80^{\circ}\text{C})$~~ $-1.09 \pm 0.93^{\circ}\text{C}$ and $-0.91 \pm 0.80^{\circ}\text{C}$, respectively. These basins had few areas with MAGT_{15m} ~~values~~ $< -3^{\circ}\text{C}$, with only 0.4% and 0.2% of the area falling below this threshold. Conversely, a substantial proportion had MAGT_{15m} ~~values~~ $> -1.5^{\circ}\text{C}$, at 73.2% and 80.3%, respectively. The MAGT_{15m} values were slightly higher eastward in the Yangtze and Yellow ~~River-river~~ basins, with averages of $-0.92 \pm 0.74^{\circ}\text{C}$ and $-0.80 \pm 0.61^{\circ}\text{C}$, respectively. The standard deviations in these basins were below 1°C . Less than 0.2% of the area had MAGT_{15m} ~~values~~ $< -3^{\circ}\text{C}$, whereas the majority had MAGT_{15m} ~~values~~ $> -1.5^{\circ}\text{C}$, accounting for 81.8% and 87.9%, respectively.

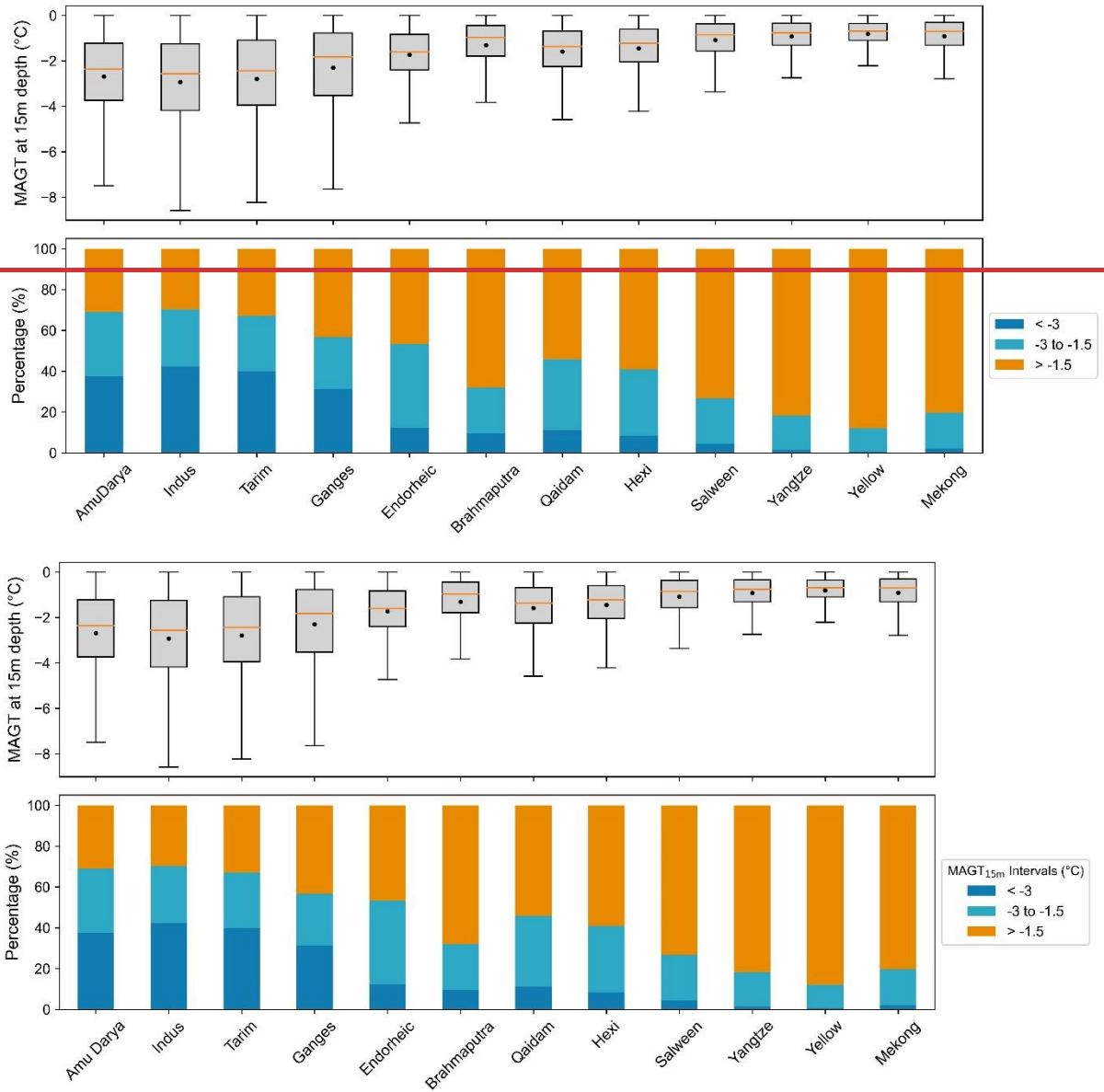


Figure 7: Distribution (a) and percentage of area in three intervals (b) of MAGT at 15 m depth (MAGT_{15m}) in 12 basins of the Qinghai-Tibet Plateau during 2010-2019.

4 Discussion

265 The SVR method exhibited more scattered predictions in the low-temperature range compared to the high-temperature range, as illustrated in Figure 3. While performing well in the high-temperature range with slight overestimations, the SVR method may potentially result in some degree of underestimation in regions with lower temperatures. This variability could be

attributed to the scarcity of MAGT_{15m} observations with colder temperature. Notably, most of the MAGT_{15m} observations utilized in this study were obtained from the eastern QTP regions, particularly the source area of the Yangtze and Yellow-River regions river, which are characterized by relatively higher MAGT_{15m} values. Additionally, the analysis suggests that the vertical lapse rate of the MAGT_{15m} increased with the-rising elevation. Hence, future monitoring efforts should prioritize cold-colder permafrost areas at higher elevations to ensure adequate representation in the study area.

We considered negative MAGT_{15m} ~~values~~ as indicators-an indicator of permafrost and estimated the permafrost area as approximately 1.36×10^6 km² (excluding glacier and lake areas), accounting for about 44.0% of the total QTP. This finding broadly aligns with previous studies based on ~~MAGT_{dzaa}~~-MAGT_{DZAA} reporting permafrost extents of approximately 1.30×10^6 km² by Wang et al. (2020) and 1.32×10^6 km² by Zhao et al. (2024). The discrepancies may arise from differences in data samples. Our study benefited from integrating MAGT_{15m} records from 231 boreholes, providing a more comprehensive dataset in terms of spatial coverage and quantity, ensuring the reliability of our prediction. Furthermore, the estimated permafrost area within the Chinese territory of the QTP was approximately 1.11×10^6 km², comparable to values derived from the temperature at the top of the permafrost (TTOP) model (1.06 to 1.09×10^6 km²) (Zou et al., 2017; Cao et al., 2023). Differences in measurement depths and temperature values between ~~MAGT_{dzaa}~~-MAGT_{DZAA} and MAGT_{15m} may have contributed to slight variations in ~~the~~ permafrost area. Additionally, permafrost may still persist in areas where MAGT_{15m} exceeds 0 °C. Statistical analysis reveals that the areas with MAGT_{15m} within the ranges of 0-0.1 °C and 0-0.2 °C cover approximately 0.05×10^6 km² and 0.10×10^6 km², respectively.

~~Based on the classification criteria established by MAGT_{dzaa}, the permafrost can be categorized into three types: cold (≤ -3.0 °C), cool (-3 to -1.5 °C), and warm (> -1.5 °C) permafrost (Ran et al., 2022). We analyzed the distribution characteristics of the QTP permafrost based on this classification system using the predicted MAGT_{15m} data. Warm permafrost was the most prevalent type in the QTP, encompassing 51.2% of the permafrost region, followed by cool permafrost (30.7%) and cold permafrost (18.1%). The forms of permafrost degradation vary depending on ground temperature regimes. Cold permafrost is characterized by rapid increased in ground temperature and slow permafrost thawing, whereas warm permafrost undergoes rapid thawing with a slower ground temperature increase (Biskaborn et al., 2019; Smith et al., 2022). This phenomenon can be attributed to the higher apparent thermal diffusivity in colder permafrost layers, where temperatures near 0 °C led to latent heat consumption by ground ice melts, resulting in lower diffusivity and less energy required to raise ground temperatures (Isaksen et al., 2011; Nicolsky and Romanovsky, 2018).~~ Based on the classification criteria established by MAGT_{DZAA}, the permafrost can be categorized into cold (≤ -1.0 °C) and warm (> -1.0 °C) permafrost (Wu et al., 2010). Using the predicted MAGT_{15m} data, we analyzed the distribution characteristics of permafrost on the QTP based on this classification. Cold permafrost was the dominant type, covering 63.7% of the permafrost regions, while warm permafrost accounted for 36.3% during the period from 2010 to 2019. The modes of permafrost degradation vary depending on ground temperature regimes (Jin et al., 2006; Wu et al., 2010). The cold permafrost tends to be more prevalent in steep alpine regions in the QTP, as

300 depicted in Figure 6. These areas typically exhibit thin surface sediment layers and shallow burial depths of bedrock. These
characteristics indicate that the degradation of cold permafrost on the QTP is primarily involves increasing ground
temperatures, particularly in regions with limited ground ice. In areas with ice-rich permafrost, the slope effect may contribute
to an increased occurrence of thaw slumps (Luo et al., 2022). Notably, a significant portion of the warm permafrost area on
the QTP is located on flat and gentle slopes, where ice-rich permafrost is often found (Zou et al., 2024). Rapid permafrost
305 thawing in these areas may increase surface deformation, resulting in ecological evolution (Jin et al., 2021), hydrological
imbalance (Walvoord and Kurylyk, 2016), and engineering stability (Ma et al., 2011). Of particular concerns are the headwater
areas of Yangtze and Yellow river basins, where warm permafrost is predominant, making these regions highly susceptible to
the impacts of short-term permafrost thaw.

~~The cold permafrost tends to be more prevalent in steep mountainous regions in the QTP, as depicted in Figure 6. These areas~~
310 ~~typically exhibit thin surface sediment layers and shallow bedrock (Shangguan et al., 2017). These characteristics indicate that~~
~~the degradation of cold permafrost in the QTP is primarily involves increasing ground temperatures, particularly in regions~~
~~with limited ground ice. In areas with ice rich permafrost, the slope effect may contribute to an increased occurrence of thaw~~
~~slumps (Luo et al., 2022). Notably, approximately half of the warm permafrost area in the QTP is located on flat and gentle~~
~~slopes (Fig. 6b), where ice rich permafrost is often found (Zou et al., 2024). Rapid permafrost thawing in these areas may~~
315 ~~increase surface deformation, resulting in ecological evolution (Jin et al., 2021), hydrology imbalance (Walvoord and Kurylyk,~~
~~2016), and engineering stability (Ma et al., 2011). Of particular concern are the Yangtze River and Yellow River basins, where~~
~~warm permafrost exceeded 80% of the area, are highly susceptible to the impacts of short term permafrost thawing. The~~
~~degradation impacts in cool permafrost areas are expected to lies between those in cold and warm permafrost areas and more~~
~~likely closer to those of the latter due to similar terrain features.~~

320 The gridded MAGT_{15m} data generated in this study represents the average ~~value-values~~ in the period from 2010 to 2019,
providing valuable boundary conditions for future permafrost dynamics ~~investigations~~ in the QTP. For instance, this data can
be leveraged in conjunction geothermal datasets to ~~estimate permafrost thickness accurately~~ more accurately estimate
permafrost thickness. Moreover, the depth-fixed MAGT baseline can serve as a robust data for validating numerical model
simulations of long-term changes in ~~the permafrost temperature field~~ permafrost temperature. These validations are crucial for
325 enhancing our understanding of QTP permafrost responses to environmental drivers and climate change. Additionally, the
MAGT_{15m} data offers critical insights for understanding geological processes and ecosystem dynamics, thereby supporting
related studies in the QTP permafrost regions.

5 Data availability

The gridded data generated by this study is publicly available and can be downloaded at the National Tibetan Plateau Data Center (TPDC) (<https://doi.org/10.11888/Cryos.tpd.301165>, Zou et al., 2024). The data in GeoTIFF format can be used with GIS software.

6 Conclusion

This study produced gridded data of ~~the mean annual ground temperature at 15 meters depth (MAGT_{15m}) during the last decade (2010-2019)~~ MAGT_{15m} during 2010-2019 at a spatial resolution of nearly 1 km in permafrost regions ~~of the Qinghai-Tibet Plateau (QTP) on the QTP~~. Regions with negative MAGT_{15m} ~~values~~ covered 1.36×10^6 km² (excluding glacier and lake areas), ~~constituting or~~ 44.0% of the QTP area. The average MAGT_{15m} was ~~-1.85 °C (±1.58 °C)~~ -1.85±1.58 °C, with 90% of values in the range of -5.1 °C to -0.1 °C and 51.2% ~~of values were higher than -1.5 °C~~ higher than -1.5 °C. The ~~freezing degree days (FDD)~~ FDD was the most significant predictor of MAGT_{15m}, followed by ~~the thawing degree days (TDD), mean annual precipitation (MAP), and soil bulk density (BD)~~ TDD, MAP, and BD. ~~The MAGT_{15m} exhibited a monotonic increase eastward, a slight decrease northward, and an accelerated decrease with increasing elevation across the QTP. Across the QTP, MAGT_{15m} exhibited a monotonous eastward increase, a slight northward decrease, and an accelerated upward decrease.~~ Lower MAGT_{15m} values were more prevalent in ~~high mountainous alpine~~ high mountainous alpine areas with steep slopes. Areas with flat and gentle slopes accounted for approximately half of both the medium (-3.0 to -1.5 °C) and high (-1.5 to 0 °C) MAGT_{15m} intervals. The lowest MAGT_{15m} values (-2.9 to -2.7 °C) were observed in the ~~basins headwater areas~~ basins headwater areas of the Amu Darya, Indus, and Tarim river basins of the western QTP. Conversely, the Yangtze and Yellow ~~River river~~ River river basins exhibited the highest ~~MAGT_{15m} values (-0.8 to -0.9 °C)~~ MAGT_{15m} (-0.9 to -0.8 °C), and more than 80% of areas were warm permafrost regions. Our gridded MAGT_{15m} dataset can serve as a valuable resource for further studies on ~~deep permafrost characteristics of the QTP~~ characteristics of elevational permafrost at greater depths of the QTP, particularly for estimating permafrost thickness.

Author contributions. DZ, LZ: conceptualization; DZ, GH, and ED: methodology; GL, WL: data processing and analysis; DZ and CW: original draft writing; LZ and GH: review and editing; LZ: supervision; LZ and GH: funding acquisition.

Competing interests. The contact author has declared that none of the authors has any competing interests.

Acknowledgements. We would like to express our gratitude to all colleagues and students for their fieldwork contributions in collecting valuable in situ data on the Qinghai-Tibet Plateau. This research was funded by the Second Tibetan Plateau Scientific

Expedition and Research (STEP) program (grant no. 2019QZKK0201) and the National Natural Science Foundation of China
355 (grant nos. 41931180 and 42322608).

References

- Aalto, J., Karjalainen, O., Hjort, J., and Luoto, M.: Statistical forecasting of current and future circum-Arctic ground temperatures and active layer thickness, *Geophys. Res. Lett.*, 45, 4889–4898, doi:10.1029/2018GL078007, 2018.
- Amatulli, G., Domisch, S., Tuanmu, M. N., Parmentier, B., Ranipeta, A., Malczyk, J., and Jetz, W.: A suite of global, cross-
360 scale topographic variables for environmental and biodiversity modeling, *Sci. Data*, 5, 180040, doi:10.1038/sdata.2018.40, 2018.
- Basak, D., Pal, S., and Patranabis, D. C.: Support Vector Regression, ~~*Neural Information Processing*, 11, 2007.~~ *Neural Information Processing—Letters and Reviews*, 11(10), 203–224, 2007.
- Biskaborn, B. K., Smith, S. L., Noetzli, J., Matthes, H., Vieira, G., Streletskiy, D. A., Schoeneich, P., Romanovsky, V. E.,
365 Lewkowicz, A. G., Abramov, A., Allard, M., Boike, J., Cable, W. L., Christiansen, H. H., Delaloye, R., Diekmann, B., Drozdov, D., Etzelmüller, B., Grosse, G., Guglielmin, M., Ingeman-Nielsen, T., Isaksen, K., Ishikawa, M., Johansson, M., Johannsson, H., Joo, A., Kaverin, D., Kholodov, A., Konstantinov, P., Kröger, T., Lambiel, C., Lanckman, J. P., Luo, D., Malkova, G., Meiklejohn, I., Moskalenko, N., Oliva, M., Phillips, M., Ramos, M., Sannel, A. B. K., Sergeev, D., Seybold, C., Skryabin, P., Vasiliev, A., Wu, Q., Yoshikawa, K., Zheleznyak, M., and Lantuit, H.: Permafrost is warming
370 at a global scale, *Nat. Commun.*, 10, 1–11, doi:10.1038/s41467-018-08240-4, 2019.
- Cao, B., Zhang, T., Peng, X., Mu, C., Wang, Q., Zheng, L., Wang, K., and Zhong, X.: Thermal characteristics and recent changes of permafrost in the upper reaches of the Heihe River Basin, western China, *J. Geophys. Res.*, 123, 7935–7949, doi:10.1029/2018JD028442, 2018.
- Cao, Z., Nan, Z., Hu, J., Chen, Y., and Zhang, Y.: A new 2010 permafrost distribution map over the Qinghai-Tibet Plateau
375 based on subregion survey maps: a benchmark for regional permafrost modeling, *Earth Syst. Sci. Data*, 15, 3905–3930, doi:10.5194/essd-15-3905-2023, 2023.
- Dobinski, W.: Permafrost, *Earth-Sci. Rev.*, 108, 158–169, doi:10.1016/j.earscirev.2011.06.007, 2011.
- Fick, S. E. and Hijmans, R. J.: WorldClim 2: new 1-km spatial resolution climate surfaces for global land areas, *Int. J. Climatol.*, 37, 4302–4315, doi:10.1002/joc.5086, 2017.
- 380 Jin, H., Zhao, L., Wang, S., and Jin, R.: Thermal regimes and degradation modes of permafrost along the Qinghai-Tibet Highway, *Sci. China Ser. D-Earth Sci.*, 49, 1170–1183, doi.org/10.1007/s11430-006-2003-z, 2006.
- Jin, X., Jin, H., Iwahana, G., Marchenko, S. S., Luo, D., Li, X., and Liang, S.: Impacts of climate-induced permafrost degradation on vegetation: A review, *Adv. Clim. Chang. Res.*, 12, 29–47, doi:10.1016/j.accre.2020.07.002, 2021.

- Li, J., Sheng, Y., Wu, J., Wang, J., Zhang, B., Ye, B., Zhang, X., and Qin, X.: Modeling regional and local-scale permafrost distribution in Qinghai-Tibet Plateau using equivalent-elevation method, *Chin. Geogr. Sci.*, 22, 278–287, doi:10.1007/s11769-012-0520-6, 2012.
- Li, J., Sheng, Y., Chen, J., Wu, J., and Wang, S.: Variations in permafrost temperature and stability of alpine meadows in the source area of the Datong River, northeastern Qinghai-Tibet Plateau, China, *Permafrost-Permafr. Periglac.*, 25, 307–319, doi:10.1002/ppp.1822, 2014.
- Li, J., Sheng, Y., Wu, J., Feng, Z., Ning, Z., Hu, X., and Zhang, X.: Landform-related permafrost characteristics in the source area of the Yellow River, eastern Qinghai-Tibet Plateau, *Geomorphology*, C, 104–111, doi:10.1016/j.geomorph.2016.06.024, 2016.
- Liu, G., Xie, C., Zhao, L., Xiao, Y., Wu, T., Wang, W., and Liu, W.: Permafrost warming near the northern limit of permafrost on the Qinghai-Tibetan Plateau during the period from 2005 to 2017: A case study in the Xidatan area, *Permafrost-Permafr. Periglac.*, 32, 323–334, doi:10.1002/ppp.2089, 2021.
- Liu, J. and Shi, R.: Characteristics of permafrost development in Jingyangling Pass of National Highway 227, Qinghai Province, *Highway*, 64, 75–80, 2019 (in Chinese).
- Luo, D., Jin, H., Lin, L., He, R., Yang, S., and Chang, X.: New progress on permafrost temperature and thickness in the source area of the Huanghe River, *Sci. Geogr. Sin.*, 32, 898–904, 2012 (in Chinese).
- Luo, D., Jin, H., Lin, L., You, Y., Yang, S., and Wang, Y.: Distributive features and controlling factors of permafrost and the active layer thickness in the Bayan Har Mountains along the Qinghai-Kangding Highway on northeastern Qinghai-Tibet Plateau, *Sci. Geogr. Sin.*, 33, 635–640, 2013 (in Chinese).
- Luo, D., Jin, H., Jin, X., He, R., Li, X., Muskett, R. R., Marchenko, S. S., and Romanovsky, V. E.: Elevation-dependent thermal regime and dynamics of frozen ground in the Bayan Har Mountains, northeastern Qinghai-Tibet Plateau, southwest China, *Permafrost-Permafr. Periglac.*, 29, 257–270, doi:10.1002/ppp.1988, 2018.
- Luo, D., Jin, H., Marchenko, S. S., and Romanovsky, V. E.: Difference between near-surface air, land surface and ground surface temperatures and their influences on the frozen ground on the Qinghai-Tibet Plateau, *Geoderma*, 312, 74–85, doi.org/10.1016/j.geoderma.2017.09.037, 2018.
- Luo, J., Niu, F., Lin, Z., Liu, M., Yin, G., and Gao, Z.: Inventory and frequency of retrogressive thaw slumps in permafrost region of the Qinghai-Tibet Plateau, *Geophys. Res. Lett.*, 49, e2022GL099829, doi:10.1029/2022GL099829, 2022.
- Ma, W., Mu, Y., Wu, Q., Sun, Z., and Liu, Y.: Characteristics and mechanisms of embankment deformation along the Qinghai-Tibet Railway in permafrost regions, *Cold Reg. Sci. Technol.*, 67, 178–186, doi:10.1016/j.coldregions.2011.02.010, 2011.
- Obu, J., Westermann, S., Barboux, C., Bartsch, A., Delaloye, R., Grosse, G., Heim, B., Hugelius, G., Irrgang, A., Kääb, A., Kroisleitner, C., Matthes, H., Nitze, I., Pellet, C., Seifert, F., Strozzi, T., Wegmüller, U., Wiczorek, M., and Wiesmann, A.: ESA Permafrost Climate Change Initiative (Permafrost_cci): Permafrost ground temperature for the Northern Hemisphere (v3.0), doi:10.5285/b25d4a6174de4ac78000d034f500a268, 2021.

- Poggio, L., de Sousa, L. M., Batjes, N. H., Heuvelink, G. B. M., Kempen, B., Ribeiro, E., and Rossiter, D.: SoilGrids 2.0: producing soil information for the globe with quantified spatial uncertainty, *SOIL Soil*, 7, 217–240, doi:10.5194/soil-7-217-2021, 2021.
- 420 Qiu, Y., Guo, H., Chu, D., Zhang, H., Shi, J., Shi, L., Zheng, Z., and Laba, Z.: MODIS daily cloud-free snow cover product over the Tibetan Plateau(V3), Science Data Bank, <https://datapid.cn/31253.11.sciencedb.55>, 2021.
- Ran, Y., Li, X., Cheng, G., Nan, Z., Che, J., Sheng, Y., Wu, Q., Jin, H., Luo, D., Tang, Z., and Wu, X.: Mapping the permafrost stability on the Tibetan Plateau for 2005–2015, *Sci. China Earth Sci.*, 64, 62–79, doi:10.1007/s11430-020-9685-3, 2021.
- 425 Ran, Y., Li, X., Cheng, G., Che, J., Aalto, J., Karjalainen, O., Hjort, J., Luoto, M., Jin, H., Obu, J., Hori, M., Yu, Q., and Chang, X.: New high-resolution estimates of the permafrost thermal state and hydrothermal conditions over the Northern Hemisphere, *Earth Syst. Sci. Data*, 14, 865–884, doi:10.5194/essd-14-865-2022, 2022.
- Romanovsky, V. E., Smith, S. L., and Christiansen, H. H.: Permafrost thermal state in the polar Northern Hemisphere during the international polar year 2007–2009: a synthesis, *Permafrost Permafr. Periglac.*, 21, 106–116, doi:10.1002/ppp.689, 2010.
- 430 Smith, S. L., Romanovsky, V. E., Lewkowicz, A. G., Burn, C. R., Allard, M., Clow, G. D., Yoshikawa, K., and Throop, J.: Thermal state of permafrost in North America: a contribution to the international polar year, *Permafrost Permafr. Periglac.*, 21, 117–135, doi:10.1002/ppp.690, 2010.
- Smith, S. L., O’Neill, H. B., Isaksen, K., Noetzli, J., and Romanovsky, V. E.: The changing thermal state of permafrost, *Nat. Rev. Earth Environ.*, 3, 10–23, doi:10.1038/s43017-021-00240-1, 2022.
- 435 Sun, Z., Ma, W., Mu, Y., Liu, Y., Zhang, S., and Wang, H.: Permafrost change under natural sites along the Qinghai-Tibet railway during the years of 2006–2015, *Adv. Earth Sci.*, 33, 248–256, 2018 (in Chinese).
- Walvoord, M. A. and Kurylyk, B. L.: Hydrologic impacts of thawing permafrost—A review, *Vadose Zone J.*, 15, vzj2016.01.0010, doi:10.2136/vzj2016.01.0010, 2016.
- Wang, D., Wu, T., Zhao, L., Mu, C., Li, R., Wei, X., Hu, G., Zou, D., Zhu, X., Chen, J., Hao, J., Ni, J., Li, X., Ma, W., Wen, A., Shang, C., La, Y., Ma, X., and Wu, X.: A 1 km resolution soil organic carbon dataset for frozen ground in the Third Pole, *Earth Syst. Sci. Data*, 13, 3453–3465, doi:10.5194/essd-13-3453-2021, 2021.
- 440 Wang, H., Zhan, J., Wang, C., Liu, W., Yang, Z., Liu, H., and Bai, C.: Greening or browning? The macro variation and drivers of different vegetation types on the Qinghai-Tibetan Plateau from 2000 to 2021, *Front. Plant Sci.*, 13, 1045290, doi:10.3389/fpls.2022.1045290, 2022.
- 445 Wang, T., Yang, D., Yang, Y., Piao, S., Li, X., Cheng, G., and Fu, B.: Permafrost thawing puts the frozen carbon at risk over the Tibetan Plateau, *Sci. Adv.*, 6, eaaz3513, doi:10.1126/sciadv.aaz3513, 2020.
- Wu, J., Sheng, Y., Wu, Q., and Wen, Z.: Processes and modes of permafrost degradation on the Qinghai-Tibet Plateau, *Sci. China Ser. D-Earth Sci.*, 53, 150–158, doi.org/10.1007/s11430-009-0198-5, 2010.
- 450 Wu, Q., Zhang, T., and Liu, Y.: Permafrost temperatures and thickness on the Qinghai-Tibet Plateau, *Global Glob. Planet. Change*, 72, 32–38, doi:10.1016/j.gloplacha.2010.03.001, 2010.

- Zhang, G., Luo, W., Chen, W., and Zheng, G.: A robust but variable lake expansion on the Tibetan Plateau, *Sci. Bull.*, 64, 1306–1309, doi:10.1016/j.scib.2019.07.018, 2019.
- Zhao, L., Wu, Q., Marchenko, S. S., and Sharkhuu, N.: Thermal state of permafrost and active layer in Central Asia during the international polar year, *Permafrost-Permafr.* Periglac., 21, 198–207, doi:10.1002/ppp.688, 2010.
- 455 Zhao, L., Zou, D., Hu, G., Wu, T., Du, E., Liu, G., Xiao, Y., Li, R., Pang, Q., Qiao, Y., Wu, X., Sun, Z., Xing, Z., Sheng, Y., Zhao, Y., Shi, J., Xie, C., Wang, L., Wang, C., and Cheng, G.: A synthesis dataset of permafrost thermal state for the Qinghai–Tibet (Xizang) Plateau, China, *Earth Syst. Sci. Data*, 13, 4207–4218, doi:10.5194/essd-13-4207-2021, 2021.
- Zhao, L., Hu, G., Liu, G., Zou, D., Wang, Y., Xiao, Y., Du, E., Wang, C., Xing, Z., Sun, Z., Zhao, Y., Liu, S., Zhang, Y., Wang, L., Zhou, H., and Zhao, J.: Investigation, monitoring, and simulation of permafrost on the Qinghai-Tibet Plateau: A review, *Permafrost-Permafr.* Periglac., ppp.2227, doi:10.1002/ppp.2227, 2024.
- 460 Zou, D., Zhao, L., Sheng, Y., Chen, J., Hu, G., Wu, T., Wu, J., Xie, C., Wu, X., Pang, Q., Wang, W., Du, E., Li, W., Liu, G., Li, J., Qin, Y., Qiao, Y., Wang, Z., Shi, J., and Cheng, G.: A new map of permafrost distribution on the Tibetan Plateau, *The Cryosphere*, 11, 2527–2542, doi:10.5194/tc-11-2527-2017, 2017.
- Zou, D., Zhao, L., Hu, G., Du, E., Liu, G., Wang, C., and Li, W.: Permafrost temperature baseline at 15 meters depth in the Qinghai–Tibet Plateau (2010–2019), *National Tibetan Plateau / Third Pole Environment Data Center*, <https://doi.org/10.11888/Cryos.tpdc.301165>, 2024.
- 465 Zou, D., Pang, Q., Zhao, L., Wang, L., Hu, G., Du, E., Liu, G., Liu, S., and Liu, Y.: Estimation of permafrost ground ice to 10 m depth on the Qinghai-Tibet Plateau, *Permafrost-Permafr.* Periglac., ppp.2226, doi:10.1002/ppp.2226, 2024.